EXAMINATION OF THE INFLUENCE OF EMPIRIC PARAMETERS ON THE AERO-ACOUSTIC RESULTS OF THE FREE WAKE CODE FIRST

Patrick P. Kranzinger, Manuel Keßler, and Ewald Krämer

Institute of Aerodynamics and Gas Dynamics (IAG), University of Stuttgart
Pfaffenwaldring 21, 70569 Stuttgart, Germany
kranzinger@iag.uni-stuttgart.de

Abstract

Due to society's increased noise sensitivity and enhanced certification requirements for new helicopters, free wake methods recently experience a revival. In combination with todays increased available computing power free wake methods allow fast and efficient aero-acoustic prediction of BVI flight situations. Within the recent years at IAG the free wake method FIRST has been developed, which can be weakly coupled to flight mechanic tools such as CAMRAD II and (G)HOST. By means of a BVI forward descent flight state, a parameter study is conducted examining the influences of the spatial and temporal discretization, and of the vortex core size on the aerodynamic and aero-acoustic solution. The underlying systematics are identified and an efficient parameter strategy for future simulation setups is proposed.

1 NOTATION

Ψ	rotor azimuth
BVI	blade vortex interaction
BPF	blade passing frequency
CAA	Computational Aero-Acoustics
CFD	Computational Fluid Dynamics
CSD	Computational Structure Dynamics
EPNL	Effective Perceived Noise Level
FW-H	Ffowcs Williams-Hawkings
GP	ground plate
MR	main rotor
PNLT	tone corrected Perceived Noise Level
R	rotor radius
r_c	vortex core radius
$\frac{r}{R}$	relative blade radial station
SPL	Sound Pressure Level
TAS	true air speed

2 INTRODUCTION

The continuous increase of available computing power and enhanced certification requirements for new helicopters in terms of noise emission have recently led to a revival of free wake methods for aero-acoustic prediction. In the past, low fidelity free wake methods already showed good qualitative agreement on resolving the blade vortex interaction phenomenon (BVI)[1]. BVI mainly occurs during slow descent flights when the rotor blades interact with the blade tip vortices of the preceding blade convecting through the rotor plane. Slicing the vortices leads to strong local load fluctuations and consequently strong unpleasant pulsating noise is emitted.

Recently, progress has been made in the field of higher order methods and the power of today's high performance computation clusters. This allows for a more accurate prediction of the aero-acoustic footprint of helicopters by CFD solvers[2][3]. Nevertheless, enormous computational power is required to investigate even a single flight case.

For rotor system design purposes, a fast and reliable prediction tool is required, that allows for the investigation of several configurations under the constraints time and costs. By increasing the spatial and temporal discretization density, the reliability of free wake methods, their prediction quality, and agreement with CFD results and experimental data is being improved to meet these demands. In fact, this makes free wake methods a first choice when BVI noise estimation is required in conjunction with limited computing resources or for exploration of large design spaces.

In recent years, the Free wake IAG Rotor Simulation Tool (FIRST) has been developed by the Institute of Aerodynamics and Gas Dynamics, which allows fast examination of different rotor and complete helicopter configurations with regard to BVI noise. The aerodynamic and aero-acoustic prediction capability of our tool chain combined with the newly developed free wake solver FIRST was validated by Kranzinger et al.[4] previously. For this purpose, a slow, 6° forward descent BVI flight situation of the Airbus Helicopters' H145 main rotor was investigated and compared to recently published CFD computations and experimental data.

To substantiate the first validation results, to quantify the influence of empiric parameters on the solution, and to define reference values for the input parameters, a parameter study is conducted. The influence of the temporal and spatial discretization on the aeroacoustic results is investigated. Additionally, as free wake methods require semi empiric modeling of viscous effects within the core of vortices, the influence of the selected viscous vortex core radius is also examined.

3 METHODS

3.1 Free wake

FIRST is a stand-alone aerodynamics solver for multirotor systems based on the instationary potential theory. For stationary, three-dimensional, and frictionless cases, e. g. for a stationary forward flight of fixed wing aircrafts, the wake can be modeled by a continuous chordwise vorticity distribution representing the spanwise gradient of the local lift, featuring two strong tip vortices. In instationary situations, e. g. for maneuver flight of a fixed wing aircraft or the forward flight of a helicopter, the upstream conditions of the wings respectively of the rotor blades are continuously changing. Thus, the local lift distribution underlies a temporal variation that leads to changes of the vorticity distribution of the wake.

Contrary to some simple stationary cases, no analytical solution is known. Hence, the problem needs to be discretized and solved numerically. Therefore, FIRST uses a spatial discretization in spanwise direction of the wake. The vorticity layer is modeled by discrete linear vortex filaments, whose edge points are freely convecting in space due to the induction of all other elements. For each time step the currently induced velocity at the endpoints of each filament is computed. The wake development is then achieved by time integration using an explicit 5^{th} order Predictor-Corrector scheme based on the Adams-Bashforth and Adams-Moulton method.

The disregard of friction would lead to physically impossible high flow speeds close to discrete vortex filaments, for which reason vortex core models are used to stabilize the method and express the induced velocity correctly. FIRST is featuring the Rankine, Scully and Vatistas vortex models[5] [6] [7] [8]. Additionally, neglecting friction leads to the total absence of dissipation. Thus, the lack of an empiric dissipation model results in a constant vortex strength of each filament of the wake. FIRST supports vortex dissipation and aging models.

The numeric complexity of free wake methods is $O({n_{trailer}}^2)$, respectively $O\left(\left(T_{simulation,\ max}/\Delta t_{time\ step}\right)^2\right)$. Using one node (featuring 24 cores) of the HLRS super computing cluster *Hazel Hen*, currently about 5 h are required to complete one rotor revolution of the setup used as basis for the parameter study (compare table 2). Beside the application of Fast Multi Pole methods, the best strategy to accelerate the solution is to reduce the number of vortex filaments taken into account.

FIRST features vortex aggregation and dropping on the basis of their distance to defined areas of interest. This allows a variable reduction of the resolution with increasing distance to the components investigated, without losing absolute energy conserved within the flow field.

FIRST features lifting line, lifting surface, and lifting body models as well as pure displacers (like a fuselage). Movements of different structure components, as e.g. blades and the fuselage, are represented by a freely configurable motion tree. The code is Shared Memory Parallelized using POSIX threads on the intranode level and uses MPI for inter-node communication.

Linking against IAG-developed libraries, which are used for structure deformation and load evaluation[9] [10], provides interfaces for automated weak and strong coupling to different computational structure dynamics (CSD) and flight mechanics tools (as e.g. CAMRAD II[11] or (G)HOST[12]). The weak coupling tool chain is completed by the helicopter coupling controlling tool HeliCats[13].

3.2 Flight Mechanics (FM) and Structural Dynamics (CSD)

For helicopter applications, a proper reproduction of the flight state including the aero-elasticity of the rotor blades is mandatory. Especially in forward flight, blade elasticity influences the aerodynamic behavior and force generation substantially.

At IAG, the structural deformation of the rotor blades is modeled using the Comprehensive Analytical Model of Rotorcraft Aerodynamics and Dynamics (CAMRAD II) code as part of a weak coupling scheme: CAMRAD II provides solutions for the blade deformation and flight kinematics, modeling the rotor blades as Euler-Bernoulli beams with isotropic material and elastic axes. For aerodynamic load estimations a low-fidelity aerodynamics model based on lifting line theory and two dimensional steady airfoil data tables is used. The initial deformation and trim-angle values are used for performing a CFD based aerodynamic simulation, providing load results of high fidelity. By correcting the internal low-fidelity loads evaluation of CAMRAD II with the CFD results, the CSD internal aerodynamics are successively replaced by the CFD, respectively free wake based loads. This leads to blade dynamics based on CFD/free wake loads with deformation and deflection calculated with CSD.

In order to fit the specified global forces and moments, an isolated rotor needs to be trimmed by applying the wind-tunnel trim scheme. The collective and the two cyclic control angles are thereby determined, while the rotor's orientation is fixed. For a complete helicopter, three additional degrees of freedom are taken into account for the spatial fuselage orientation and the tail rotor thrust. This approach is known as a free-flight trim.

3.3 Aero-acoustics (CAA)

For computing the aero-acoustic noise emission, the IAG developed CAA code ACCO[14] is used. The absolute load distribution along the quarter chord of every rotor blade over time serves as basis for the computation. Therefore, the resulting pressure fluctuations at the surface of the rotor blades are reduced to local force vectors by sectional integration within every time step.

Acoustic modeling is achieved by using the Ffowcs-Williams-Hawkings (FW-H) equation

$$\frac{\overline{\partial}^2 \overline{\rho}'}{\partial t^2} - c^2 \overline{\nabla}^2 \rho' = \frac{\partial}{\partial x_i}[p' n_i \delta(f)] + \frac{\partial}{\partial t}[\rho_0 v_n \delta(f)] \tag{1}$$

where $\overline{\rho}'$ is the time averaged density fluctuation, p the pressure fluctuation, n_i the normal vector, v_n the normal component of the surface velocity, and $\delta(f)$ the Dirac delta function.

By using the wave equation on the left hand side and Lighthill's acoustic analogy, undisturbed free-stream conditions are assumed for the complete volume. The right hand side of the equation represents the source terms. As FIRST is a potential flow solver, only load fluctuations (dipoles) can be directly provided. Noise emissions resulting from volume displacement are directly computed within ACCO using a three-dimensional surface mesh of the rotor blades and corresponding movement information.

As free wake methods are based on potential theory, no quadrupole source terms mainly resulting from shear layer influences or turbulence and compression shocks can be taken into account. Usually, for helicopter rotor simulations of flight states generating BVI noise, only a neglicible part of the resulting aero-acoustic emission is allotted to quadrupole terms. In the considered BVI flight state, the main noise emission can be traced back to load fluctuations on the surface of the rotor blades.

Having the FW-H equation solved, time domain acoustic pressure can be calculated at arbitrary locations in space, called observers. Finally, the specific aero-acoustic values such as narrow-band spectra, Sound Pressure Level (SPL) and Perceived Noise Level (PNL) are derived from the acoustic pressure information.

4 VALIDATION TEST CASE

Predicting aero-acoustic emissions for BVI flight states is one of the most critical applications of free wake methods with regards to their accuracy, as slight misplacements of the tip vortices have strong influence on the aero-acoustic results. Thus, it is very promising that FIRST showed its capability to predict the position of the tip vortices and their strength within the rotor disk area very robustly and accurately right from the beginning of the validation process[4].

As the main application will be the prediction of noise generated by BVI, a certification relevant slow forward descent flight state has been chosen for validation. As specified within the helicopter noise certification rules and regulations[15], three microphones are placed in a line perpendicular to the flight path on the ground with a distance of 150 m between each other. As schematically illustrated in Figure 1, the helicopter follows its 6° descent flight path orthogonally to the microphone array with a flight speed equal to the speed at its best rate of climb. Thereby, the center microphone is overflown at an altitude of 120 m.

Contrary to the noise certification procedure, the experimental data is recorded using microphones that are placed above ground plates (compare Figure 2).

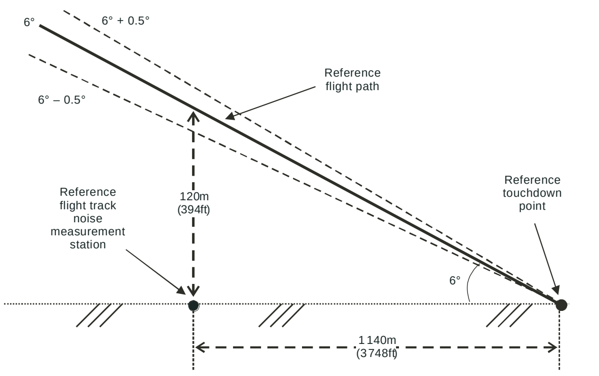

Figure 1. Schematic overview to the flight boundaries of the approach test conditions[15].

Attribute	
Rotor blades	4
Rotor radius	5.5 m
Rotor rpm	96.6 %
TAS	70 kn
Flight path angle	6.0 °
Hight over microphones	120 m
EPNL (ICAO)	90.3 EPNdB

Table 1. Main attributes of the H145 MR geometry and of the flight test conditions and results.

So the signal experiences a well-defined total reflection on the ground plate (GP). This can be approximated during evaluation by doubling pressure time signals derived from the simulations. Aero-acoustic key values are computed according to the ICAO evaluation procedure. For the evaluation, the microphone signals are considered as measured in form of pressure-time signals.

The aerodynamic and aero-acoustic results are compared to experimental flight test data recorded during the noise measurement campaign of the H145 in 2012[16]. Table 1 summarizes the main attributes of the H145 main rotor as well as the averaged testing conditions. Regarding further numerical investigations, wind speed data is not taken into account.

5 TRIMMING

For validation purposes, only the main rotor of the H145 is considered. To achieve comparable results and to enable the analyzation of only the immediate influence of the investigated parameters on the flow field and the aero-acoustic response, all computations executed for the parameter study use the same deformation information, resulted from the last trim iteration of the trim validation setup presented by Kranzinger et al.[4].

The rotor has been modeled using a lifting surface for each rotor blade with 25 vortex trailers attached. The temporal resolution has been chosen at 2 ° per time step. For evaluating the wake, the Rankine vortex model has been applied with a vortex core radius of 25 mm in combination with a 5$^{\text{th}}$ order Adams-Bashforth scheme. To get a reference solution with as little influence parameters as possible, no vortex filament aggregation, no filament dropping based on the corresponding vortex strength, and no dissipation model has been applied. The filaments have been cut off about 1.5 rotor diameters behind the rotor center. Based on experience for forward flight conditions, the filaments have left the rotor's influence area at this point.

The isolated rotor setup has been weakly coupled to CAMRAD II using the wind tunnel trim scheme. HeliCats has been used to control the complete trim process. Convergence has been achieved after eight trim runs. With a deviation of 0.8 ° for the cyclic pitch angles and 2.3 ° for the collective pitch angle in comparison to the experimental data, all resulting trim angles lie within the combined confidence interval of the experimental data and the FM model[4].

6 PARAMETER STUDY

For industrial rotor system design purposes the efficiency of numerical methods is crucial, as in general only limited computational resources are available. Due to the method complexity, it is essential to determine an optimal parameter set in terms of computational effort and aero-acoustic prediction accuracy. On this account, the influence of the main method parameters is examined.

Besides the discretization of the lift generating and displacing structures, the temporal and spatial discretization, the chosen vortex core model and its empiric coefficients are the only free parameters of free wake models. Regarding the investigated forward flight state, dissipation becomes only significant when the wake has already left the influence area of the rotor. Hence, vortex dissipation and aging have no noticeable influence on the solution and are consequently disabled to further reduce the number of empiric parameters.

To keep the influence of the modeling of the rotor blades themselves as small as possible, the lifting surfaces are only adapted when the spatial resolution and consequently the number of trailers is varied. If the spanwise discretization of the lifting surface has not been adapted, a vortex strength aggregation model would have been used, which would lead to a whole bunch of additional empiric parameters.

Finally, the parameter study is separated into three separate investigations examining the influence of the

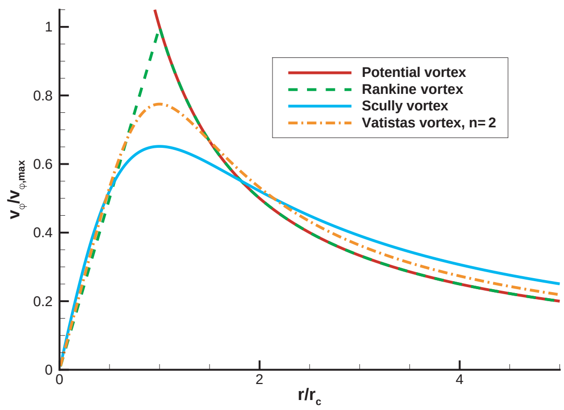

Figure 2. Comparison of the induced tangential velocity of different vortex core models.

spatial discretization (number of trailers), of the temporal discretization (time step size), and of the viscous vortex core size. Experience show that the influence of the chosen vortex core model on the aero-acoustic solution is insignificant. As it can be seen in Figure 2, the main parameter of all vortex core models specifies the area where the vorticity dominates and leads to solid rotation. The influence of vortex core size variations dominates the minor differences in terms of induced velocity in the blending area between potential vortex and solid rotation. Thus, the usage of the Rankine vortex model is sufficient regarding the investigation of the correlation of vortex core size variations with the resulting noise emission.

Table 2 shows the reference values chosen for the parameter study. These values are based on experience gained during the development process of FIRST and were also used for the aero-acoustic solution in[4]. Solutions using these values showed qualitatively and quantitatively good agreement with experimental data and CFD solutions. The results of the parameter study are assessed by means of the relative deviation of the rotor thrust to the reference solution (ct. table 2). For aero-acoustic analysis, the delta EPNL values of the center microphone are compared to experimental data.

For the investigated flight state, BVI occurs both at the advancing blade between $\Psi = 45°$ and $\Psi = 110°$ and the retreating blade between $\Psi = 255°$ and $\Psi = 330°$. In contrast to the BVI events at the advancing side, the events on the retreating side generate primarily noise emissions, which emit to the top[2]. Consequently, only the BVI events at the advancing side dominate the helicopter's noise footprint and are investigated in detail in the subsequent sections.

Attribute	
Number of trailers per blade	50
Time step size	1°
Vortex core radius	100 mm
ΔEPNL value	–0.96 EPNdB
(Compared to experiment.)	
ΔRotor thrust	*(reference)*

Table 2. Reference values of varied parameters, and aerodynamic and aero-acoustic key values.

Originally, free wake methods only provide vortex filament locations in space and corresponding strengths. Detailed investigations of vortex locations and locally aggregated vortex strength are challenging especially for densely discretized evaluations. The native plots only consist of discrete lines in space, where coloring may be used for indicating the individual vortex filament strength. To get a better overview of the detailed structure of the flow field, for the area of main interest in terms of BVI (azimuthal area of $\Psi = 20°$ to $\Psi = 120°$ at radial position $r/R = 0.75$) the vortex strength and location has been rendered on a discretized cylindric plane. Therefore, the vortex strength of each filament has been blended to an influence radius of 100 mm

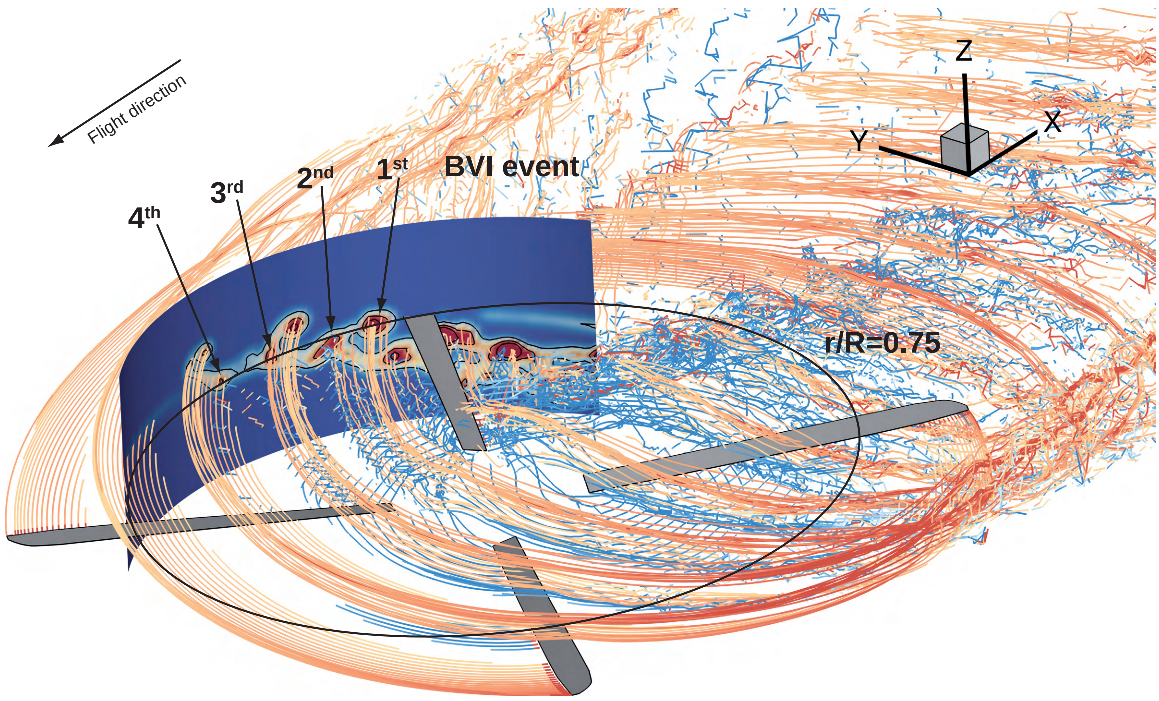

Figure 3. Vortex trailers and cylinder slice with aggregate vortex strength.
($\Psi = 50°$; 200 mm vortex core radius; 50 trailers per rotor blade; 1° temporal resolution.)

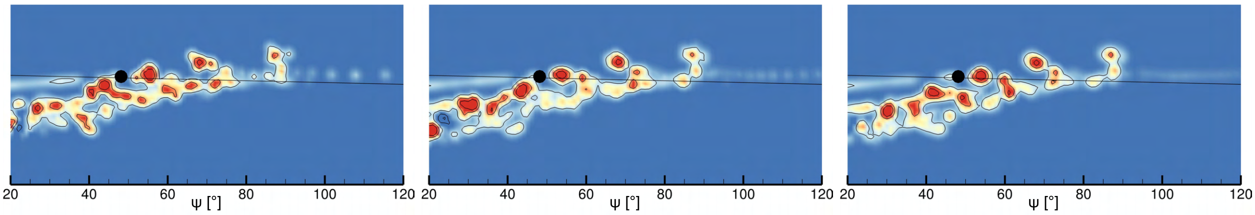

(a) 25 vortex trailers

(b) 50 vortex trailers

(c) 100 vortex trailers

Figure 4. Vortex locations at $r/R = 0.75$ **shortly before occurrence of first BVI-event.**
(Rotor blade position $\Psi = 50°$**;** 100 mm **vortex core radius;** 1° **temporal resolution.)**

using Gaussian distribution. Subsequently, this individual local vortex influence value is summed up for all vortex filaments at each node of the cylinder (compare Figure 3). By unrolling the cylinder fragment, a 2D contour plot results, which gives a good overview of the location and strength of the major vortex structures.

Figure 3 shows that only the first and strongest BVI event is triggered by a direct interaction of the rotor blade with a blade tip vortex–precisely with the blade passed 1¼ revolutions ago. All following BVI events result from interaction with the rolled up vortex layer.

6.1 Influence of spatial discretization

First of all, the influence of the spanwise discretization is investigated. Therefore, the vortex core size and the temporal discretization are kept constant at 100 mm and 1° respectively.

Figures 6(a), 7(a) and 8(a) show the lift distribution for a complete revolution. There is almost no deviation of the absolute value. All main features are present in all configurations. For 25 trailers, the azimuthal area between $\Psi = 60°$ and $\Psi = 120°$ shows less smooth and unexpected lift fluctuations in comparison with the 50 and 100 trailers solutions. In addition to that, the rearward area (between $\Psi = 330°$ and $\Psi = 30°$) shows a slightly higher thrust.

The azimuthal (temporal) derivative of the local lift coefficients shown in Figures 6(b), 7(b) and 8(b) show similar characteristics: For all configurations, the areas of strong azimuthal local lift gradients are similarly located, which can be reasoned with similar positions in space of the BVI generating vortex structures. However, for the 25 trailers solution the second and third BVI event is strongly scattered and not sufficiently represented. This can be traced back to the coarse spatial resolution of both, the lifting surface panels and the wake vortex layer.

The total vortex strength of the wake generated by the rotor blades correlates with the total rotor thrust. Consequently, it is (mostly) independent of the spatial resolution. By discretizing a rotor blade's wake with less trailers, the strength of each individual vortex trailer increases. As the vortex core size is not adapted to the reduced spanwise resolution, the maximum possible induced velocity increases. Hence, trailers which pass the rotor blade next to collocation points induce a significant higher downward velocity. The local lift of each lifting surface panel is computed only based on the velocity induced at its collocation point. The obtained pressure value is applied to the complete panel area, which has also grown in spanwise direction. Based on both effects, local lift fluctuations are consequently overrated.

Figure 4 gives an overview of the vortex locations and the corresponding strengths. The black dot is placed at the actual position of the rotor blade's $c/4$-line. The slightly sloping black line shows the intersection of the cylinder slice with the effective rotor plane. The vortex fields of the 50 and 100 trailer solutions show almost no difference. Neither the strength nor the position of the vortex centers differ perceptibly. Only the rolled up vortex layer being responsible for the second BVI event is more compact and consequently locally stronger in the refined case. By comparing Figure 7(a) and Figure 8(a), again no deviation can be noticed for

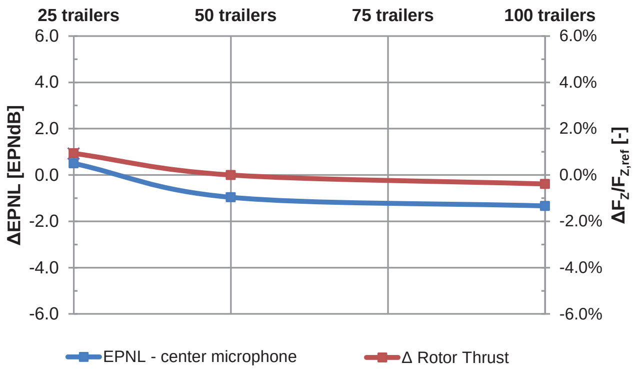

Figure 5. Development of EPNL noise levels and averaged rotor thrust by refining spatial resolution.

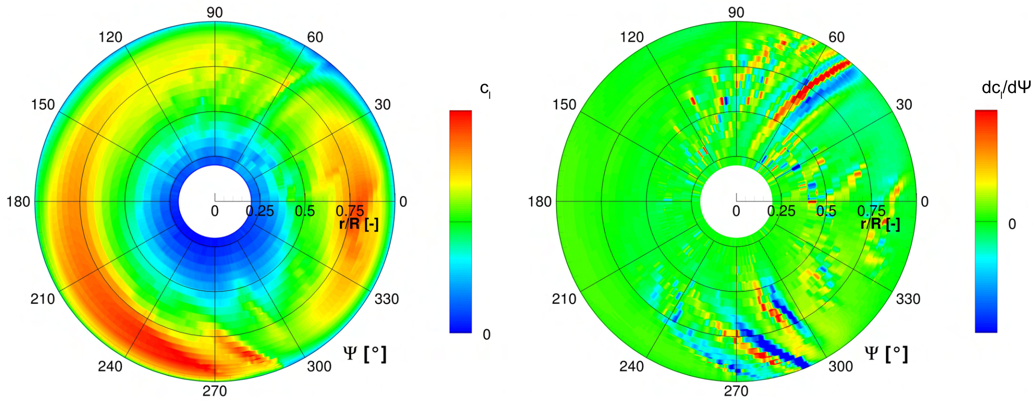

(a) Sectional lift coefficient

(b) Azimuthal (time) derivative of the sectional lift coefficient

Figure 6. 100 mm **vortex core radius,** 25 **trailers,** 1 ° **temporal resolution.**

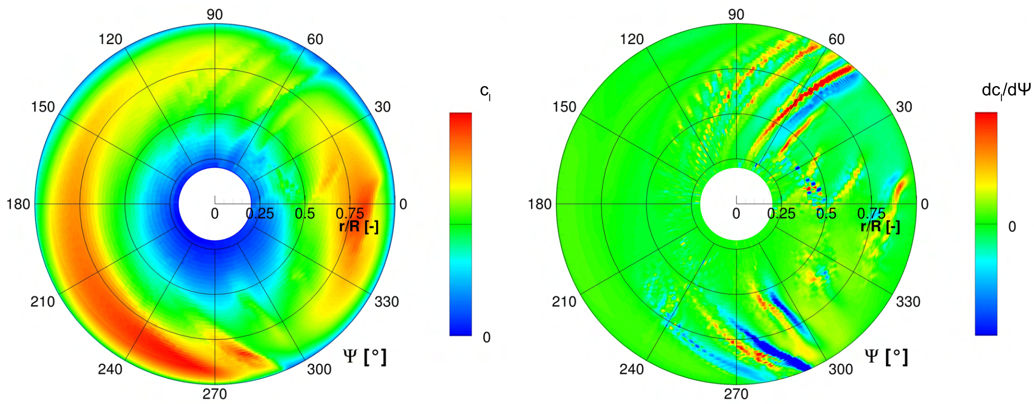

(a) Sectional lift coefficient

(b) Azimuthal (time) derivative of the sectional lift coefficient

Figure 7. 100 mm **vortex core radius,** 50 **trailers,** 1 ° **temporal resolution.**

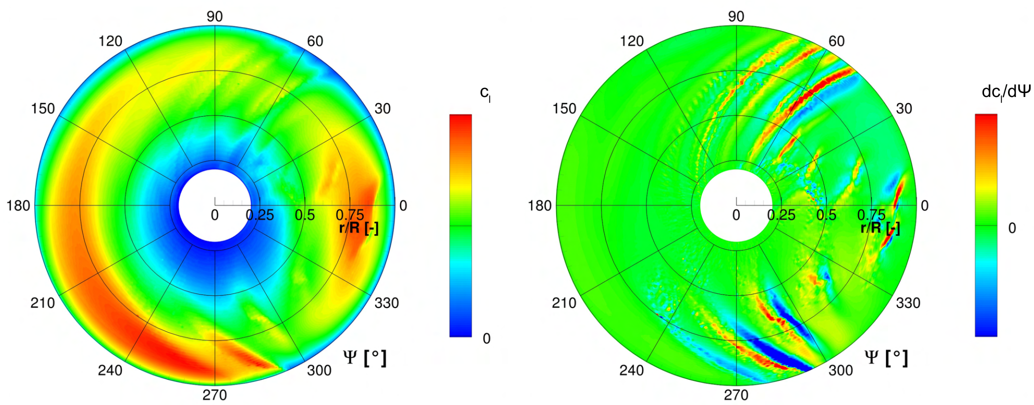

(a) Sectional lift coefficient

(b) Azimuthal (time) derivative of the sectional lift coefficient

Figure 8. 100 mm **vortex core radius,** 100 **trailers,** 1 ° **temporal resolution.**

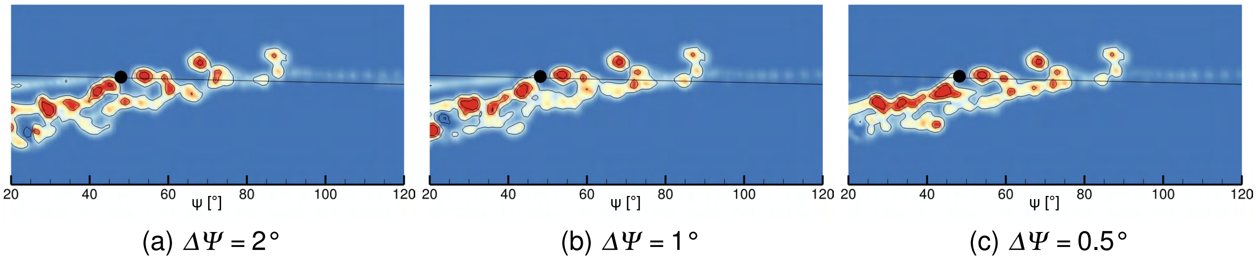

Figure 9. Vortex locations at $r/R = 0.75$ **shortly before occurrence of first BVI-event.**
(Rotor blade position $\Psi = 50°$**;** 100 mm **vortex core radius;** 50 **trailers per blade.)**

the lift gradients. In contrast, the 25 trailers solution shows significant differences. The main vortex structures are still located at the correct positions and with correct strength, but the secondary vortex structures reflecting the roll-up of the vortex layer and causing the second and third BVI event (compare Figure 3) are misplaced and partly overestimated. This results from the concentration of the constant total wake vortex strength to not enough trailers.

The aerodynamic thrust is slightly increasing by reducing the number of trailers to 25. Due to the overestimation of the secondary vortex structures the EPNL value is increased by ca. 1.5 EPNdB. Both values behave convergent when the spatial discretization is refined. The same examination has also been conducted for a reduced vortex core radius of 25 mm showing the same trend–qualitatively and quantitatively. Computations with 45 trailers and 55 trailers fit the thrust's and noise emission's logarithmic regression, as well: The deviation is only ± 0.6 EPNdB in term of noise, respectively ± 0.1 percent in terms of thrust.

Summing up, at least about 50 trailers are required to achieve good aero-acoustic results, whereas no significant improvement is achieved using additional trailers. Consequently, a 50 trailers setup seems to be a good compromise in terms of numerical effort and outcome. Further optimization can be achieved by improving the distribution function used for placing the trailers to better fit the local requirements along the spanwidth: The circulation attached to trailers corresponds with the local spanwise lift gradient. Areas with strong spanwise lift gradient require a denser discretization, as the vorticity layer generated here tends to roll up and form strong BVI relevant vortex structures as shown in Figure 3. In contrast, trailers leaving the blade in areas with low spanwise lift gradients have no significant influence on the solution, which is why the discretization can be chosen coarser within these areas.

6.2 Influence of temporal discretization

The impact of the temporal discretization is also investigated on basis of the reference setup (50 trailers, 100 mm vortex core radius, compare Table 2) by halving and doubling the time step size to 0.5° respectively 2.0°.

Figure 9 shows the vortex placement and corresponding strength of all investigated temporal discretization levels. Again, nearly no difference between the three solutions can be seen. The vortex structure generating the second BVI event seems to be slightly overrated for the coarsest computation case, whereas all relevant vortices are similarly positioned for all solutions. Due to the high order extrapolation scheme, an increase of the time step size to 2° has no relevant influence on the vortex layer roll-up behavior and consequently on the vortex placement. Experience obtained during the development phase of FIRST showed that the reduction of the computation scheme order to three or less massively increases the method sensitivity in terms of time step size.

By comparing the lift distribution on the rotor plane no significant differences can be found (compare Figures 11(a), 12(a), and 13(a)), whereas the azimuthal

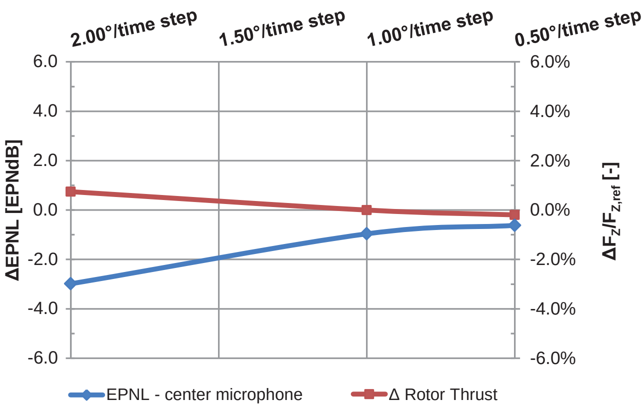

Figure 10. Development of EPNL noise levels and averaged rotor thrust by refining temporal resolution.

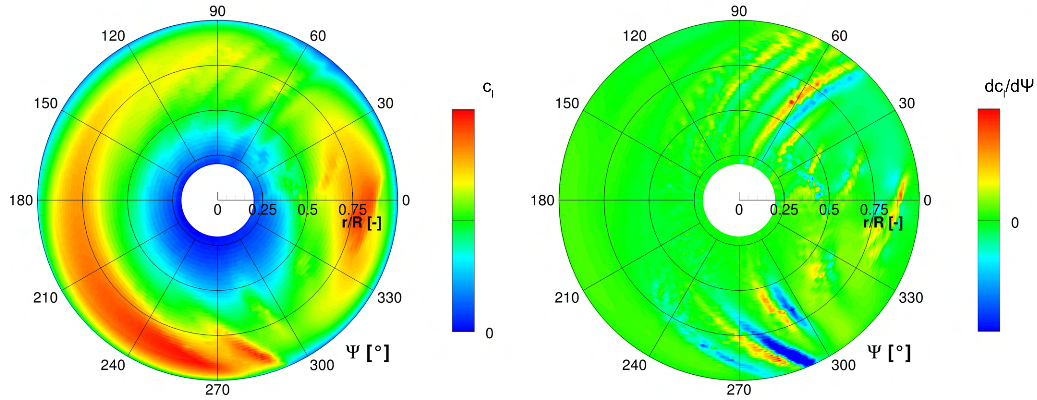

(a) Sectional lift coefficient

(b) Azimuthal (time) derivative of the sectional lift coefficient

Figure 11. 100 mm **vortex core radius,** 50 **trailers,** 2 ° **temporal resolution.**

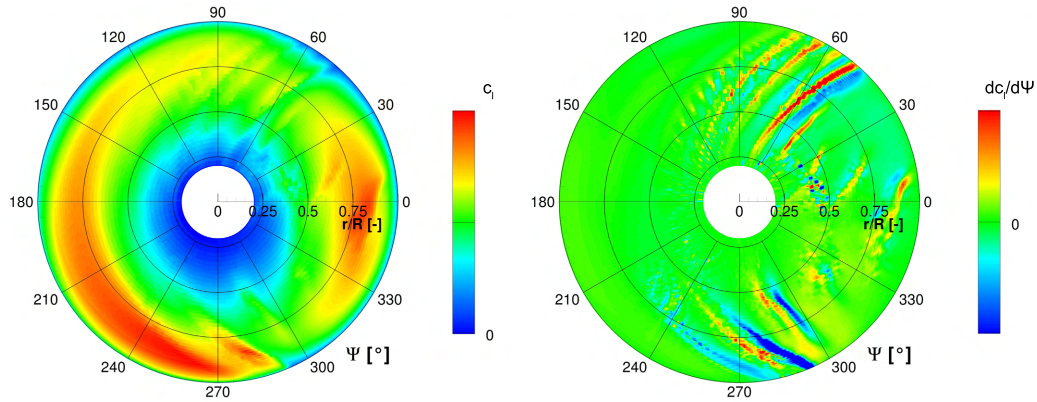

(a) Sectional lift coefficient

(b) Azimuthal (time) derivative of the sectional lift coefficient

Figure 12. 100 mm **vortex core radius,** 50 **trailers,** 1 ° **temporal resolution.**

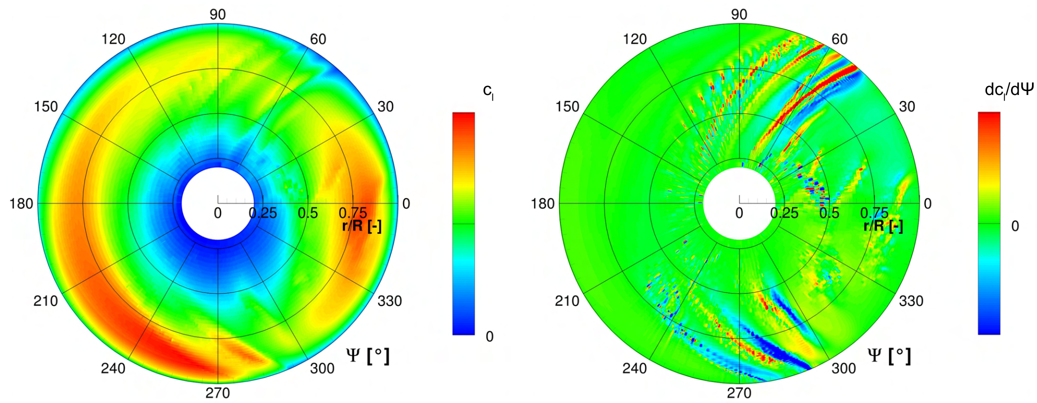

(a) Sectional lift coefficient

(b) Azimuthal (time) derivative of the sectional lift coefficient

Figure 13. 100 mm **vortex core radius,** 50 **trailers,** 0.5 ° **temporal resolution.**

(temporal) derivation of the local lift of the 2° solution shows significant artifacts. This indicates temporal underdiscretization (compare Figures 11(b), 12(b), and 13(b)). As expected, the refined solution shows more details and sharper BVI events with slightly stronger lift gradients.

Comparing the $dc_l/d\Psi$-plots with the corresponding CFD solution published by Kowarsch et al.[2], which has been conducted with a temporal resolution of 0.25°, it can be determined that with increasing temporal resolution the lift gradient structures are adapting.

Figure 10 shows the consequences of time step variation to the total averaged rotor thrust and to the aero-acoustic emissions of the rotor. From a aerodynamic-only point of view a 2° time step is completely fair, as the influence to the rotor thrust is only 0.7%. Contrary to that, at least a 1° time step is required, to get an adequate aero-acoustic resolution. If coarser time stepping is used, the locally occurring temporal gradients of the local lift are blurred, which results in aero-acoustic underprediction of the BVI noise.

6.3 Influence of the vortex core size

In contrast to the temporal and spatial discretization, the vortex core size is an empirical parameter, which has a direct influence on the physical solution. As its influence does not need to necessarily follow a single trend, a wide spectrum is investigated. Young has shown that the physical vortex core size r_c behind a helicopter rotor blade lies between 10^{-2} and $10^{-3}R$[17]. To get a spanwise resolution representing a continuous vortex layer trailing the helicopter rotor blades, the distance between vortex trailers needs to be in the size of the vortex core radius which correlates to 100-1000 spanwise trailers. If less trailers are used, either the core size needs to be increased to non-physical values or the velocity field behind the rotor blade is not smooth anymore. Due to the method complexity, increasing the number of trailers has a significant influence on the computation time required for running the simulation. However, experience shows, that even with 15 trailers or less and vortex core sizes greater than 150 mm good aero-acoustic agreement can be achieved[1]. As it can be seen in Figure 3 even the usage of vortex core radii of 200 mm or more do not eliminate the underdiscretization of the flow field completely, as due to roll-up some areas remain, where the vortex filament distance is far higher.

Based on the reference solution (compare Table 2), the vortex core size is varied in a range starting with the absolute minimum to get a trimmable setup: 12.5 mm up to 500 mm, which guarantees a smooth periodic solution featuring wide correctly discretized wake areas.

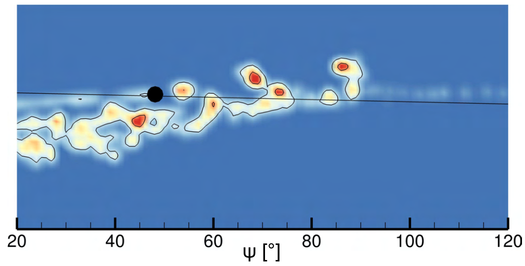

(a) 25.0 mm vortex core radius

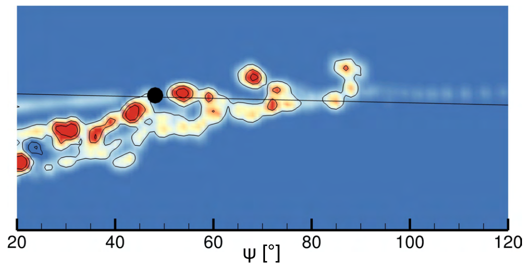

(b) 100.0 mm vortex core radius

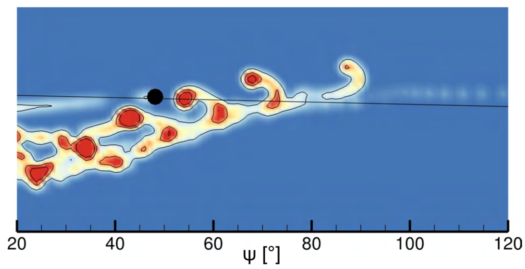

(c) 300.0 mm vortex core radius

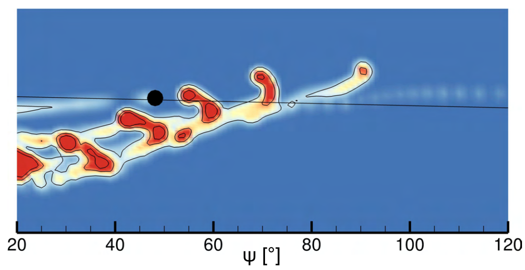

(d) 500.0 mm vortex core radius

Figure 14. Vortex locations at $r/R = 0.75$ shortly before occurrence of first BVI-event.
(Rotor blade position $\Psi = 50°$; 50 trailers per blade; 1° time step duration.)

As shown in Figure 14, in the range between 12.5 mm and 100 mm the effective vortex strengths strongly correlate with the vortex core size. When the vortex core radius is reduced below 100 mm the blade tip vortices and the areas where the wake vortex layer is rolling up forming secondary vortex structures show massive degeneration caused by underdiscretization. This leads to stochastically occurring unphysically high velocity peaks at the end points of vortex filaments when passing others. As a result, shortly

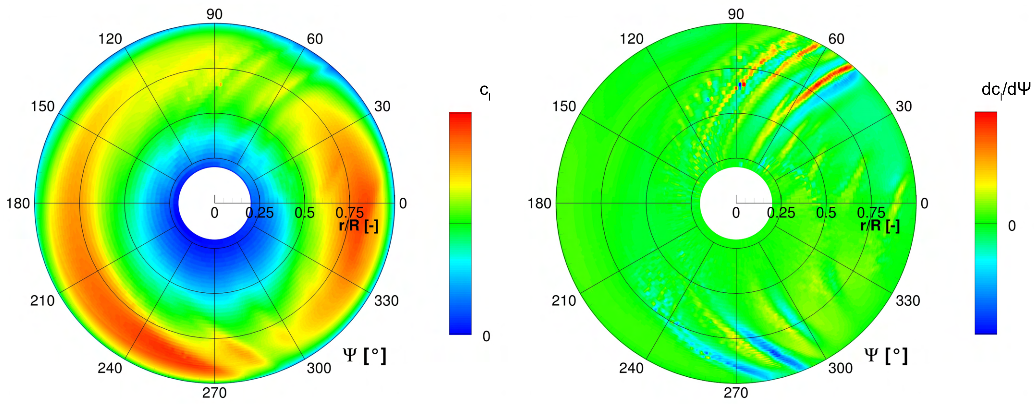

(a) Sectional lift coefficient

(b) Azimuthal (time) derivative of the sectional lift coefficient

Figure 15. 25 mm **vortex core radius,** 50 **trailers,** 1 ° **temporal resolution.**

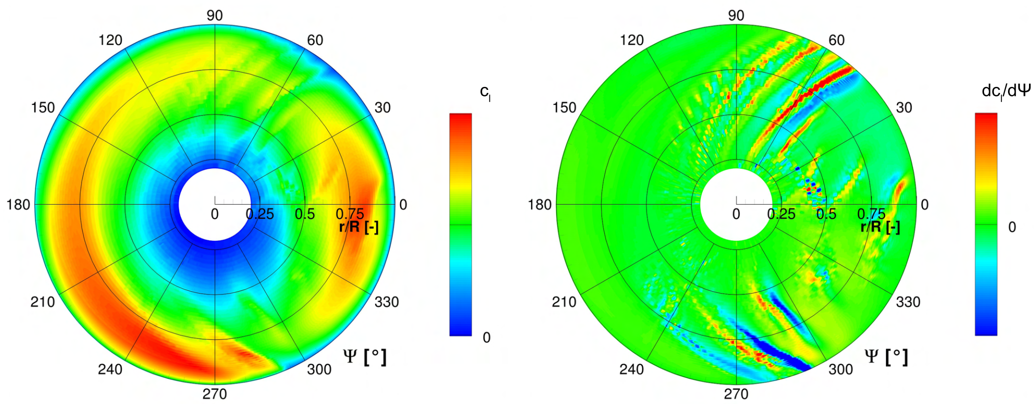

(a) Sectional lift coefficient

(b) Azimuthal (time) derivative of the sectional lift coefficient

Figure 16. 100 mm **vortex core radius,** 50 **trailers,** 1 ° **temporal resolution.**

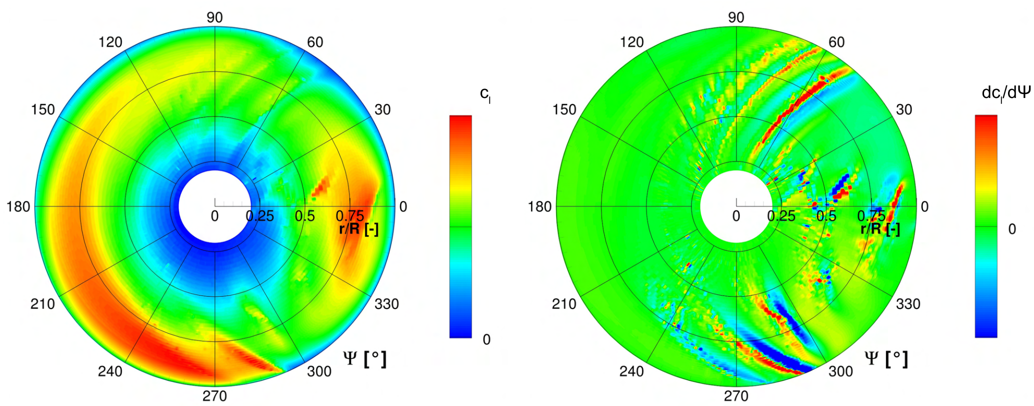

(a) Sectional lift coefficient

(b) Azimuthal (time) derivative of the sectional lift coefficient

Figure 17. 300 mm **vortex core radius,** 50 **trailers,** 1 ° **temporal resolution.**

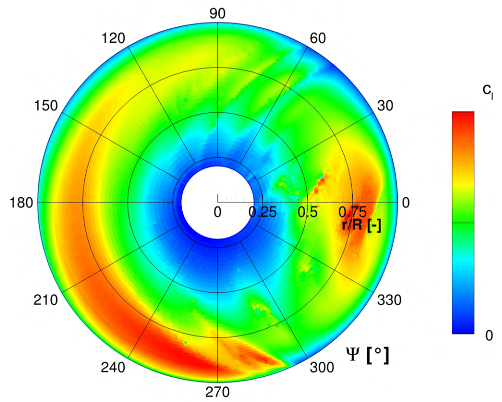

(a) Sectional lift coefficient

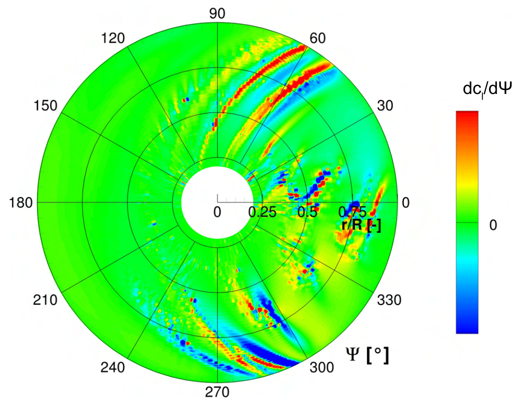

(b) Azimuthal (time) derivative of the sectional lift coefficient

Figure 18. 500 mm **vortex core radius,** 50 **trailers,** 1 ° **temporal resolution.**

after wake evolution starts, vortex filaments, which should be oriented unidirectionally, have messed up and cancel each other out. This leads to a reduced aggregate vortex strength. A side effect can also be seen in Figures 15(a), 16(a), 17(a), 18(a), which show the local lift coefficient: The area with higher local lift generation between Ψ = 330 ° and Ψ = 30 ° is much clearer contoured for bigger vortex core sizes as the aggregated strength of the rotor disc boundary vortices is higher as well as the induced downward velocities. The higher induced velocities also explain the drop of lift when the viscous vortex core size is increased (compare Figure 19).

Additionally, a reduced aggregated vortex strength leads to less compact vortex structures as in turn the intensity of the roll-up process is dependent on the maximal induced velocities within the vortex cores, which directly depend on the local strength of vorticity.

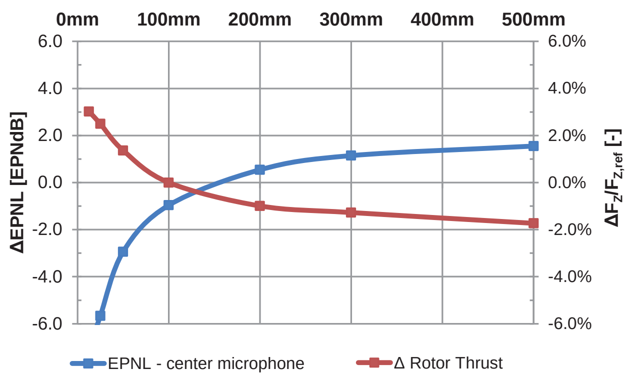

Figure 19. Development of EPNL noise levels and averaged rotor thrust by vortex core size variations.

Figures 15(b), 16(b), 17(b), 18(b) show the azimuthal (temporal) derivative of the local lift coefficient. The decrease of the aggregated vortex strength that is caused by the decrease of the core radii can be clearly seen by means of the lower temporal lift gradients. Due to the mess up of the vortex structures, not all of the originally chordwise directed vortex filaments are striking the subsequent rotor blades' surfaces with the same angle at the same time. This reduces their influence on the locally occurring loads. On this account, as shown in Figure 19 the aero-acoustic evaluation shows lower EPNL values.

Increasing the viscous vortex core too far leads to an underestimation of local flow field features, as the upper limit of the induced velocities drops. The roll-up of small, energetically intensely, actually physically correct structures is prevented. Comparing the vortex locations of the last tip vortex structure for the 100 mm and 500 mm solution already shows a significant misplacement of the fourth, light BVI event. (compare Figure 14(b), 14(d)). By trend, aero-acoustic phenomena would be underpredicted. The influence on global aerodynamic loads would be much less significant as they mainly depend on the large main structures of the flow field as e. g. the aggregated rotor disc boundary vortices.

Considering the aero-acoustic results in comparison to the experimental data, the intensity of the BVI relevant vortices and their location relative to the rotor disc is optimal for a viscous vortex core size between 100 mm and 200 mm. Typically, the vortex core radius should be chosen in the same size as the average spanwise trailer distance. For the 5.5 m radius of H145 main rotor and 50 trailers per rotor blade, the average trailer distance is 110 mm, hereby confirming these findings.

7 CONCLUSIONS

The parameter study showed that varying the discretization parameters mainly influences the strength of the developing main vortex structures being responsible for BVI. Their location and convection are only affected marginally. The temporal discretization is primarily important with regard to the lift evaluation on the blades. Too large time steps make for underpredicting the local lift gradients and consequently the noise emitted. An adequate spatial discretization is required for correct representation of the vortex structure generation itself. If too few trailers are placed behind a rotor blade, at one hand the blade tip vortex is not being kept compact. At the other hand, the vortex strength distribution is not reflected exactly enough to allow an accurate prediction of the roll-up of the secondary vortex structures being responsible for the second, third and fourth BVI event. In addition, because of physical reasons, the strength of the vortex layer keeps constant, but is now distributed to a less number of discrete vortex filaments. These effects–a wider spread of the blade tip vortices, a more random convection of the filaments, and the higher filament individual vortex strength–lead to a slight overprediction of the noise generated by the BVI events, if the number of trailers per blade drops below 50.

In contrast, the vortex core size influences the macroscopic geometric evolution of the flow field. If it is decreased too far, measured on the spatial discretization level, unphysical high velocity peaks arise within the wake, which lead to stochastic movement of the filament end points. This causes mutual cancellation and consequently a lower aggregate vortex strength. However, the main structures are still correctly located and convecting. If the vortex core size is increased too far, the collocation points within the close-up range of a vortex filament are moved too slowly. The velocity induced within the vortex core is, because of its size, massively underpredicted. Consequently, the roll-up process occurs too inertly, leading to an underdeveloped wake. The parameter study confirms the literature statement, that the vortex core radius should match the average vortex filament distance of the wake, as long as the discretization can not be chosen finer than the physical vortex core radius.

Summing up, FIRST behaves as expected on parameter variations and variations of the simulated flight situations. All parameter variations showed strongly converging behavior, which confirms the robustness and reliability of the code. For future aerodynamic only, respectively trim computations, a 50 trailers setup with an increased time step size of 2° and a vortex core radius of 150 mm seems to be the most efficient setup. Therefore, in a next step the influence of a further increase of the time step size is investigated. In contrast, for aero-acoustic simulations the usage of a 50 trailers setup with a vortex core radius of 150 mm but with an increased temporal resolution of at least 1° per time step is adequate and leads to good agreement with experimental data.

The next upcoming milestones of the validation process are the application of these findings to more flight cases and rotor systems and the confirmation of the acceleration techniques. The accurate prediction of noise emissions in combination with its robustness and performance makes FIRST a trustable and powerful tool within industrial rotor design processes.

Acknowledgments

This work was performed within the BMWi (Federal Ministry of Economics and Technology) funded federal research project FTEG-ECO-HC2, grant number 20H0803.

The authors would like to thank Airbus Helicopters Deutschland GmbH for the esteemed cooperation within this project and beyond, as well as for providing us with experimental data to enable this investigation.

Further acknowledgement is made to the High Performance Computing Center in Stuttgart who provided us with support and service to perform the computations on their high performance computing system Hazel Hen.

REFERENCES

[1] Zerle, L., *Aerodynamische und aeroakustische Rotorberechnung unter Anwendung frei entwickelter Nachlaufwirbelschichten und retardierter Potentiale*, Ph.D. thesis, Institut für Aerodynamik und Gasdynamik, Universität Stuttgart, 2000.

[2] Kowarsch, U., Lippert, D., Schneider, S., Keßler, M., and Krämer, E., "Aeroacoustic Simulation of an EC145T2 Rotor in descent flight", 71th American Helicopter Society Annual Forum, Virginia Beach, VA, 2015.

[3] Kowarsch, U., Öhrle, C., Keßler, M., and Krämer, E., "Aeroacoustic Simulation of a complete EC145T2 Helicopter in descent flight", 41th European Rotorcraft Forum, Munich, Germany, 2015.

[4] Kranzinger, P., Keßler, M., and Krämer, E., "Aeroacoustic Validation of the Free Wake Method FIRST on the Basis of a H145 Main Rotor in Descent Flight", 42th European Rotorcraft Forum, Lille, France, 2016.

[5] Rankine, W., *A Manual of Applied Mechanics*, Charles Griffin and Company, 1872.

[6] Kaufmann, W., "Über die Ausbreitung kreiszylindrischer Wirbel in zähen Flüssigkeiten", *Ingenieur-Archiv*, Vol. 13, (1), 1962.

[7] Scully, M. P. and Sullivan, J. P., "Helicopter Rotor Wake Geometry and Airloads and Development of Laser Doppler Velocimeter for Use in Helicopter Rotor Wakes", Technical Report DSR No. 73032, Massachusetts Institute of Technology Aerophysics Laboratory, Cambridge, MA, 1972.

[8] Vatistas, G., Kozel, V., and Mih, W., "A simpler model for concentrated vortices", *Experiments in Fluids*, Vol. 1, (11), 1991, pp. 73–76.

[9] Schuff, M., Kranzinger, P. P., Keßler, M., and Krämer, E., "Advanced CFD-CSD Coupling: Generalized, High Performant, Radial Basis Function Based Volume Mesh Deformation Algorithm for Structured, Unstructured and Overlapping Meshes", 40th European Rotorcraft Forum, Southampton, UK, 2014.

[10] Kranzinger, P., Kowarsch, U., Schuff, M., Keßler, M., and Krämer, E., "Advances in Parallelization and High-fidelity Simulation of Helicopter Phenomena", *High Performance Computing in Science and Engineering '15*, edited by W. E. Nagel, D. H. Kröner, and M. M. Resch, Springer International Publishing, 2015, pp. 479–494.

[11] Johnson, W., *CAMRAD II Comprehensive analytical model of rotorcraft aerodynamics and dynamics*, fourth edition, 2009.

[12] Benoit, B., Kampa, K., von Grunhagen, W., Basset, P.-M., and Gimonet, B., "HOST, a General Helicopter Simulation Tool for Germany and France", *Proceedings of the 56th Annual Forum of the American Helicopter Society*, Vol. 56, (2), 2000, pp. 1110–1131.

[13] Dietz, M., Schimke, D., and Embacher, M., "Advanced Industrial Application of CFD for Helicopter Development", Proceedings of the 36th European Rotorcraft Forum, Paris, France, September 2010.

[14] Keßler, M. and Wagner, S., "Source-Time Dominant Aeroacoustics", *Computers & Fluids*, Vol. 33, 2004, pp. 791–800.

[15] International Civil Aviation Organization, Environmental, *Technical Manual - Volume I: Procedures for the Noise Certification of Aircraft*, doc. 9501 edition, 2012.

[16] Gareton, V., Gerais, M., and Heger, R., "Acoustic Design and Testing of the Eurocopter EC145T2 and EC175B - a harmonized Franco-German Approach", 39th European Rotorcraft Forum, Moscow, 2013.

[17] Young, L., "Vortex Core Size in the Rotor Near-Wake", Technical Report NASA/TM-2003-212275, A-03010293, NASA Ames Research Center; Moffett Field, CA, 2003.